

Feature-Enhanced Synthetic Aperture Radar Image Formation Based on Nonquadratic Regularization

Müjdat Çetin, *Student Member, IEEE*, and William Clem Karl, *Senior Member, IEEE*

Abstract—We develop a method for the formation of spotlight-mode synthetic aperture radar (SAR) images with enhanced features. The approach is based on a regularized reconstruction of the scattering field which combines a tomographic model of the SAR observation process with prior information regarding the nature of the features of interest. Compared to conventional SAR techniques, the method we propose produces images with increased resolution, reduced sidelobes, reduced speckle and easier-to-segment regions. Our technique effectively deals with the complex-valued, random-phase nature of the underlying SAR reflectivities. Efficient and robust numerical solution is achieved through extensions of half-quadratic regularization methods to the complex-valued SAR problem. We demonstrate the performance of the method on synthetic and real SAR scenes.

Index Terms—Computed imaging, half-quadratic regularization, image reconstruction, inverse problems, nonquadratic optimization, regularization, synthetic aperture radar.

I. INTRODUCTION

SYNTHETIC aperture radar (SAR) is a microwave sensor which is capable of producing high-resolution images of the earth's surface. A SAR system sends electromagnetic pulses from a radar mounted on an airborne or spaceborne platform to a particular area of interest on the ground and records the return signals. In order to achieve high cross-range resolution, SAR collects data from multiple observation points, and focuses the received information coherently to obtain a high-resolution description of the scene. The all-weather nature, high resolution, and large area coverage rates of the SAR phenomenology have led to its increased use in surveillance, as well as growing interest in automated processing techniques, wherein features extracted from the formed imagery are used for automatic target detection and recognition.

There are two distinct modes in which a SAR imaging system can operate: stripmap-mode SAR, and spotlight-mode SAR. In stripmap-mode SAR, the antenna remains fixed with respect to the radar platform so that the antenna beam sweeps out a strip on the ground. In spotlight-mode, the antenna is steered to continuously illuminate a single spot of terrain. We focus on spotlight-mode SAR in this paper. The conventional technique for the formation of spotlight-mode SAR imagery is the polar format algorithm [1],

[2]. This approach while straightforward, has certain shortcomings. First, the resolution of the formed images is limited by the SAR system bandwidth. This complicates point scatterer localization for automated recognition tasks. In addition, the images suffer from speckle and sidelobe artifacts. These artifacts complicate region segmentation for shape-based recognition.

Regularization methods have been used in real-valued image restoration [3], [4], as well as image reconstruction problems such as medical tomography [5], [6] to obtain improved image estimates in the face of data degradation. The simplest and most common approach is to use quadratic functions of the unknown quantities, which leads to Tikhonov regularization [7], [8]. These methods lead to computationally straightforward optimization problems, but they suppress useful features in the resulting imagery, such as edges. Recently, considerable effort has been spent in designing alternative, nonquadratic constraints which preserve such features. Methods based on these nonquadratic constraints have been successfully used in edge-preserving regularization in image restoration [4] and computer assisted tomography [5], [6]. Unlike these standard image processing problems, SAR involves *complex-valued* reflectivities. The complex nature of SAR captures both amplitude scaling and phase shifting of the transmitted waveform by the underlying scatterers. For most SAR scenes, the phase of the reflectivity at a certain location can be modeled to be random, and uncorrelated with the phase at other locations [9]. This complex-valued nature of SAR scenes makes extension and application of real-valued regularization methods challenging.

To address these challenges, we develop a new technique for SAR image formation based on a regularized image reconstruction framework. Our method uses an explicit tomographic model relating the SAR observations to the complex-valued unknown scene. This model facilitates the incorporation of information about properties of the particular SAR sensor and measurement parameters into the processing. In addition, prior information regarding the underlying scene or features of interest are captured through a set of nonquadratic constraints on the complex field values. The resulting optimization problems can be costly, and so we present an efficient iterative method for solving such problems by extending half-quadratic optimization techniques [10], [11]. Our method provides an extension of real-valued feature-preserving image reconstruction methods [4], [5] to the SAR imaging problem. The outcomes of this approach are increased resolvability of point-scatterers, enhancement of object shapes, reduced sidelobes and reduced speckle. The method is also robust to limited quality or quantity of data.

In Section II, we briefly discuss conventional, as well as recently proposed relevant SAR image reconstruction methods.

Manuscript received May 31, 2000; revised December 15, 2000. This work was supported in part by the Air Force Office of Scientific Research under Grant F49620-96-1-0028, the National Institutes of Health under Grant NINDS 1 R01 NS34189, and the Army Research Office under Grant ARO DAAG55-97-1-0013. The associate editor coordinating the review of this manuscript and approving it for publication was Dr. Mark A. Richards.

The authors are with the Department of Electrical and Computer Engineering, Boston University, Boston, MA 02215 USA (e-mail: mcetin@bu.edu).

Publisher Item Identifier S 1057-7149(01)02475-7.

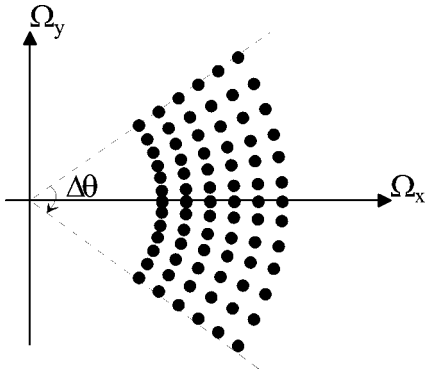


Fig. 1. Graphical representation of the observed Fourier transform samples of the reflectivity in SAR where Ω_x and Ω_y denote the spatial frequency in the x (range) and y (cross-range) directions, respectively, and $\Delta\theta$ denotes the extent of observation angles.

Section III contains necessary mathematical preliminaries, including the model of the SAR observation process used in this paper. In Section IV, we present our approach to SAR image reconstruction. Section V contains experimental results, and Section VI concludes the paper.

II. PREVIOUS WORK

The standard spotlight-mode SAR image formation algorithm, used in essentially all systems today, is the polar format algorithm [1], [2]. This algorithm is based on the fact that spotlight-mode SAR observations (after demodulation) are samples of the Fourier transform of the unknown field on a polar grid in the spatial frequency domain, as shown in Fig. 1 [1], [12]. In the polar format algorithm, the data are first interpolated to a Cartesian grid, and then an inverse two-dimensional (2-D) fast Fourier transform (FFT) is employed for image formation. Before FFT processing, the data can be windowed to reduce sidelobe levels. Another image reconstruction method, suggested by the tomographic formulation of SAR [13], is the filtered backprojection (FBP) algorithm [13]–[15]. Both the polar format and the FBP algorithms are based on the inverse operator for the case when perfect data are available throughout the spatial frequency domain. These methods have no explicit mechanism to counter any imperfection in the data. Although there are algorithmic differences between the two methods, the reconstructions they produce are very similar. We will call these methods the *conventional* methods for SAR image formation.

In conventional methods, image resolution is limited by the system bandwidth. Since peaks in the spectrum of the observed signal correspond to strong point scatterers in the scene, one idea to overcome this limit is to use modern 2-D spectral estimation methods [16] rather than a Fourier transform for forming the SAR image [17]–[20] (assuming that polar to rectangular resampling has already been done). In addition to resolution improvement, other motivations suggested for the application of these methods are to remove sidelobe artifacts, and to reduce speckle [17]. When applied to SAR imaging, spectral estimation-based methods are quite successful in preserving gain on ideal point scatterers, however most spectral estimation-based methods reduce gain on nonpointlike scatterers such as trees, and they fail to improve the quality of images containing objects

with distributed features. A comprehensive comparison of various spectral estimation methods in SAR can be found in [17]. These methods provide no explicit means to accentuate one type of feature over another.

Another way of increasing the resolution beyond the Fourier limit is to perform data extrapolation in the frequency domain by estimating samples outside the annular data region through the use of linear prediction filters [21]–[23]. There has also been some recent limited attempt to compare the performance of spectral estimation-based methods with data extrapolation-based methods. For example in [24], it has been reported that spectral estimation-based techniques have a degraded performance with real world targets (unlike with point targets), and may cause some loss of information about the target, whereas data extrapolation techniques offer increased resolution and better overall performance in these cases. On the other hand, according to [25], data extrapolation-based methods do not yield particularly good results, since they introduce significant amounts of noise.

Finally, there also exists some limited previous work taking an estimation-theoretic approach to the problem. These methods are closest in spirit to our method. In [26], a regularized inversion method has been proposed for stripmap-mode SAR, which involves deconvolution of the projections of the field by Tikhonov-type regularization, followed by backprojection. In [27], an estimation-theoretic ℓ_1 -norm-based approach has been proposed for imaging closely-spaced multiple moving scatterers over a given spatial region. Finally, a class of approaches for SAR imaging based on entropy methods has been developed [28]–[32]. These methods appear to offer good noise suppression properties, however the experimental results in published work are too limited to show other possible advantages over conventional methods. Rather than realistic SAR scenes, most results involve simple examples, such as two isolated point scatterers [28], a synthetic scene with reflectivity $1 - j$ in the target region and zero in the background (hence, not random phase) [30], [31], and a small scene consisting of straight lines and isolated point scatterers [32]. The method in [30], [31] also requires post-processing (median filtering) to reduce some of the artifacts. The recent entropy-based work in [32] considers the problem of imaging extended (distributed) targets, however the method uses smoothness constraints which are built on the real and imaginary components of the field, rather than on the magnitudes directly, unlike our approach.

III. SPOTLIGHT-MODE SAR OBSERVATION MODEL

The ground-plane geometry for spotlight-mode SAR is shown in Fig. 2. Data are collected by a radar traversing a flight path and pointing at a fixed ground patch. At points corresponding to equal angular increments, high-bandwidth pulses are transmitted and returns from the ground patch of radius L are then received and processed to form an image of the complex reflectivity field $f(x, y)$. The most commonly used pulses are linear FM chirp signals

$$s(t) = \begin{cases} e^{j(\omega_0 t + \alpha t^2)}, & |t| \leq \frac{T_p}{2} \\ 0, & \text{otherwise} \end{cases} \quad (1)$$

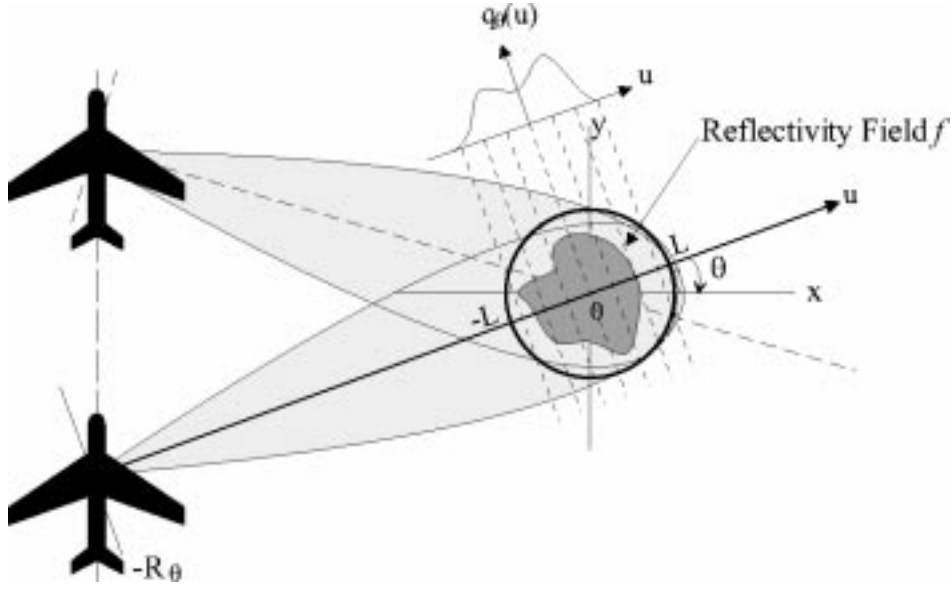


Fig. 2. Basic ground-plane geometry for spotlight-mode SAR data collection.

where ω_0 is the carrier frequency and 2α is the chirp rate. Suppose the radar transmits the real part of such a signal at the instant when the angle between the u axis and the x axis is θ , and the distance between the airplane and the center of the patch is R_θ . The return signal from the scene is mixed (multiplied) with a reference chirp signal and low-pass filtered. Assuming that $R_\theta \gg L$, so that curvature of the wavefront is negligible [13], and neglecting a quadratic phase term, the signal demodulated in this way is given by [1]

$$r_\theta(t) = \iint_{\substack{x^2+y^2 \leq L^2 \\ \cdot (x \cos \theta + y \sin \theta)}} f(x, y) \exp\{-j\Omega(t)\} \cdot dx dy. \quad (2)$$

Here, $\Omega(t) = (2/c)(\omega_0 + 2\alpha(t - (2R_\theta/c)))$ serves as the radial spatial frequency¹, and c is the speed of light. Note that $r_\theta(t)$ is a finite slice at angle θ from the 2-D Fourier transform of the field $f(x, y)$.

In practice, the observations at the i th observation angle θ_i are samples $r_{\theta_i}(t_j)$ of the continuous received signal $r_{\theta_i}(t)$ at sampling times t_j . Let \mathbf{r}_{θ_i} be the vector of these observed samples, \mathbf{C}_{θ_i} be a discretized approximation to the observation kernel in (2), and \mathbf{f} be a vector of the unknown sampled reflectivity image. Then, overall, we can write

$$\underbrace{\begin{bmatrix} \mathbf{r}_{\theta_1} \\ \mathbf{r}_{\theta_2} \\ \vdots \\ \mathbf{r}_{\theta_P} \end{bmatrix}}_{\mathbf{r}} = \underbrace{\begin{bmatrix} \mathbf{C}_{\theta_1} \\ \mathbf{C}_{\theta_2} \\ \vdots \\ \mathbf{C}_{\theta_P} \end{bmatrix}}_{\mathbf{C}} \mathbf{f} \quad (3)$$

¹Note $\Omega(t)$ is limited to a finite spatial frequency interval, because the observation duration t is limited, and the chirp rate α is finite (equivalently $s(t)$ is narrow-band). Also $\Omega(t)$ is offset from the origin of the spatial frequency plane due to ω_0 .

where P is the total number of angular observation points. The data in \mathbf{r} are the sampled phase histories, and are confined to an annular region in the spatial frequency plane as shown in Fig. 1.

By use of the projection-slice theorem [14], the observed signal $r_\theta(t)$ can also be identified as a band-pass filtered Fourier transform of the projections of the field [13]

$$r_\theta(t) = \int_{|u| \leq L} q_\theta(u) \exp\{-j\Omega(t)u\} du \quad (4)$$

where $q_\theta(u)$ is the projection at angle θ of $f(x, y)$. Based on (2) and (4), we can also obtain a discrete data relationship between the field \mathbf{f} and band-pass filtered projections. In particular, we can obtain samples of the band-pass projection information by an inverse discrete Fourier transform (IDFT) of the sampled data \mathbf{r}_{θ_i} , $i \in \{1, \dots, P\}$, at each observation angle. By stacking the results from all observation angles, we obtain

$$\bar{\mathbf{q}} = \mathbf{F}^{-1} \mathbf{r} = \mathbf{F}^{-1} \mathbf{C} \mathbf{f} = \mathbf{T} \mathbf{f} \quad (5)$$

where \mathbf{F} is a matrix whose blocks perform a DFT at each observation angle, and $\mathbf{T} = \mathbf{F}^{-1} \mathbf{C}$ represents a complex-valued discrete ‘‘SAR projection operator.’’ The data $\bar{\mathbf{q}}$ obtained in this way are the range profiles.

In the presence of noise, our model of the SAR range profile observations becomes

$$\mathbf{g} = \mathbf{T} \mathbf{f} + \mathbf{w} \quad (6)$$

where \mathbf{w} accounts for additive measurement noise. This is the relationship we will use in our method. A similar observation relationship could also be written in terms of the phase histories \mathbf{r} and the matrix \mathbf{C} , however we will use (6) in our scheme, since the sparser nature of \mathbf{T} offers computational advantages. Note that, since this system model relates reflectivities to measurements directly, we will not require polar to rectangular re-sampling.

IV. PROPOSED METHOD

We formulate the SAR image reconstruction problem as the following optimization problem

$$\hat{\mathbf{f}} = \arg \min_{\mathbf{f}} J(\mathbf{f}) \quad (7)$$

where we choose $J(\mathbf{f})$ to be an objective function of the following form:

$$J(\mathbf{f}) = \|\mathbf{g} - \mathbf{T}\mathbf{f}\|_2^2 + \lambda_1^2 \|\mathbf{f}\|_k^k + \lambda_2^2 \|\mathbf{D}\mathbf{f}\|_k^k \quad (8)$$

where $\|\cdot\|_k$ denotes the ℓ_k -norm, \mathbf{D} is a discrete approximation to the 2-D derivative operator (gradient), $|\mathbf{f}|$ denotes the vector of magnitudes of the complex-valued vector \mathbf{f} , and λ_1, λ_2 are scalar parameters. The formulation of (7), (8) starts from the observed range profiles and is not simply a post-processing of a formed image.

The first term in the objective function (8) is a data fidelity term, which incorporates the tomographic SAR observation model (6), and thus information about the observation geometry. The second and third terms in (8) incorporate prior information regarding both the behavior of the field \mathbf{f} , and the nature of the features of interest in the resulting reconstructions². These terms are aimed at enhancing point-based and region-based features respectively. The relative magnitudes of the parameters λ_1 and λ_2 determine the relative emphasis on these two types of features.

This reconstruction problem can also be obtained through Bayesian means. If we assume that the observation noise in (6) is independent identically distributed complex Gaussian noise (the most commonly used statistical model for radar measurement noise [28], [33]), and the prior probability density function for the field is given by

$$p_{\mathbf{f}}(\mathbf{f}) \propto \exp[-\mu(\lambda_1^2 \|\mathbf{f}\|_k^k + \lambda_2^2 \|\mathbf{D}\mathbf{f}\|_k^k)] \quad (9)$$

with μ a constant, then the corresponding maximum a posteriori estimate of \mathbf{f} is the solution of (7), (8). We again see that the second and third terms in (8) pertain to the inclusion of prior information. In Sections IV-A and IV-B, we will discuss in more detail the reasoning behind our particular choices for these prior information terms.

A. Enhancement of Point-based Features by $\|\mathbf{f}\|_k^k$

Many object recognition methods rely on locations of dominant point scatterers extracted from SAR images [34], [35] and one of our objectives is to produce images in which such features are enhanced. In applications such as nuclear magnetic resonance (NMR) spectroscopy [36] and astronomical imaging [37], similar objectives have previously been achieved by using maximum entropy methods. These approaches provide reconstructions with good energy concentration (i.e., most elements are small and a few are very large). It has been shown that similar behavior can be obtained using minimum ℓ_1 -norm reconstruction [38]. In spectral analysis, ℓ_k -norm constraints, where $k < 2$, have been shown to result in higher resolution spectral

²In general, the values of k used for the norms in the two prior information terms do not have to be identical. Here we use the same norm for both terms for the sake of notational simplicity.

estimates compared to the ℓ_2 -norm case (which is proportional to the periodogram) [39]. Based on these observations, we use a prior term of the form $\|\mathbf{f}\|_k^k$ with $k \leq 1$. This function imposes an energy-type constraint on the solution, and aims to suppress artifacts and increase the resolvability of scatterers. Note that a smaller value of k implies less penalty on large pixel values as compared to a larger k . This favors a field with a smaller number of dominant scatterers, and results in better preservation of the scatterer magnitudes.

From a statistical point of view, the use of a single prior term based on $\|\mathbf{f}\|_k^k$, would be equivalent to a prior model on \mathbf{f} which assumes independent identically distributed pixels with a circular³ generalized Gaussian density [40]. Two particular cases of the density would be, $k = 2$ leading to a Gaussian prior, and $k = 1$ leading to a Laplacian prior for each complex-valued pixel.

B. Enhancement of Region-Based Features by $\|\mathbf{D}\mathbf{f}\|_k^k$

SAR recognition algorithms also use region-based shape features [41], [42]. As an example, shapes of the object, shadow, and background regions are used for target classification. With conventional SAR images, segmentation of such regions is particularly difficult due to speckle. We are thus interested in reducing variability in homogeneous regions, while preserving discontinuities at region boundaries. Such behavior has been obtained in real-valued image restoration and reconstruction problems by using constraints of the form $\|\mathbf{D}\mathbf{f}\|_k^k$ with $k \approx 1$ [4], [40]. However, straightforward application of such a term to the complex-valued SAR case is problematic, since it would impose smoothness separately on the real and imaginary parts of the complex field \mathbf{f} . The correlation in a homogeneous region of \mathbf{f} in SAR is due to the similarity of backscatter power, which is better represented in the magnitude of \mathbf{f} than its real and imaginary parts. As a result, for region-based SAR imaging, we propose using the prior term $\|\mathbf{D}|\mathbf{f}|\|_k^k$. The resulting optimization problem is made much more difficult by the substitution of the term $\mathbf{D}|\mathbf{f}|$ for $\mathbf{D}\mathbf{f}$, since $|\mathbf{f}|$ is a nonlinear function of the real and imaginary parts of \mathbf{f} . Efficient and robust solution of (7) thus becomes a major challenge. In Section IV-C, we overcome this limitation by providing an efficient algorithm. Note that the advantage of region-based feature enhancement during image reconstruction rather than by post-processing a conventionally formed image is that the former is more effective in suppressing potential artifacts resulting from limitations (e.g., partial aperture) or imperfections in the data.

C. Solution of the Optimization Problem

In order to avoid problems due to nondifferentiability of the ℓ_k -norm around the origin when $k \leq 1$, we will use the following smooth approximation to the ℓ_k -norm in (8) [4]

$$\|\mathbf{z}\|_k^k \approx \sum_{i=1}^K (|\mathbf{z}_i|^2 + \epsilon)^{k/2} \quad (10)$$

where

$$\epsilon \geq 0 \text{ small constant;}$$

³Hence, phase is assumed to be uniformly distributed.

K length of the complex vector \mathbf{z} ;
 $(\mathbf{z})_i$ i th element of \mathbf{z} .

For numerical purposes, we thus will use the following slightly modified cost function

$$J_m(\mathbf{f}) = \|\mathbf{g} - \mathbf{T}\mathbf{f}\|_2^2 + \lambda_1^2 \sum_{i=1}^N (|(\mathbf{f})_i|^2 + \epsilon)^{k/2} + \lambda_2^2 \sum_{i=1}^M (|(\mathbf{D}|\mathbf{f})_i|^2 + \epsilon)^{k/2}. \quad (11)$$

Note that $J_m(\mathbf{f}) \rightarrow J(\mathbf{f})$ as $\epsilon \rightarrow 0$. The minimization of $J(\mathbf{f})$ or $J_m(\mathbf{f})$ does not yield a closed-form solution for \mathbf{f} in general, so numerical optimization techniques must be used.

Standard numerical optimization techniques like Newton's method or quasi-Newton methods with a conventional Hessian update scheme, such as DFP or BFGS [43] have been shown to perform poorly in optimization problems involving non-quadratic constraints, which are special cases of (11) [44], and we have observed this behavior as well. This precludes the use of such standard methods here. The additional presence of a constraint on the magnitude of \mathbf{f} in our case makes the problem even more difficult. To overcome these obstacles, we develop a quasi-Newton method with a new Hessian update scheme, by extending ideas from half-quadratic regularization [10] to account for the complex-valued nature of the SAR problem and the associated prior information terms. This new Hessian approximation and update strategy is matched to the structure of the SAR problem in (11). The resulting new optimization algorithm is a nontrivial extension of existing numerical schemes, and provides an efficient, robust solution.

In order to develop our scheme, we use a structure which effectively deals with both the complex-valued nature of \mathbf{f} and the nonlinearity associated with $|\mathbf{f}|$. We first take the gradient of (11) with respect to the real and imaginary parts of \mathbf{f} . This yields a gradient vector of length $2N$. We then put this vector into a compact form, by defining a complex-valued gradient vector of length N , whose real and imaginary components contain the derivatives with respect to the real and imaginary parts of \mathbf{f} respectively. This compact gradient can be placed in the following useful form following substantial manipulation

$$\nabla J_m(\mathbf{f}) = \tilde{\mathbf{H}}(\mathbf{f})\mathbf{f} - 2\mathbf{T}^H\mathbf{g} \quad (12)$$

where

$$\begin{aligned} \tilde{\mathbf{H}}(\mathbf{f}) &\triangleq 2\mathbf{T}^H\mathbf{T} + k\lambda_1^2\mathbf{A}_1(\mathbf{f}) \\ &\quad + k\lambda_2^2\boldsymbol{\Phi}^H(\mathbf{f})\mathbf{D}^T\mathbf{A}_2(\mathbf{f})\mathbf{D}\boldsymbol{\Phi}(\mathbf{f}) \\ \mathbf{A}_1(\mathbf{f}) &\triangleq \text{diag} \left\{ \frac{1}{(|(\mathbf{f})_i|^2 + \epsilon)^{1-k/2}} \right\} \\ \mathbf{A}_2(\mathbf{f}) &\triangleq \text{diag} \left\{ \frac{1}{(|(\mathbf{D}|\mathbf{f})_i|^2 + \epsilon)^{1-k/2}} \right\} \\ \boldsymbol{\Phi}(\mathbf{f}) &\triangleq \text{diag} \{ \exp(-j\phi[(\mathbf{f})_i]) \} \end{aligned} \quad (13)$$

where $\phi[(\mathbf{f})_i]$ denotes the phase of the complex number $(\mathbf{f})_i$, $(\cdot)^H$ denotes the Hermitian of a matrix, and $\text{diag}\{\cdot\}$ is a diagonal matrix whose i th diagonal element is given by the expression inside the brackets.

Examining the gradient expression (12), the term $\tilde{\mathbf{H}}(\mathbf{f})$ resembles a ‘‘coefficient’’ matrix multiplying \mathbf{f} . As a result, we use $\tilde{\mathbf{H}}(\mathbf{f})$ as an approximation to the Hessian. Note that this Hessian approximation depends on \mathbf{f} itself. We use this approximate Hessian $\tilde{\mathbf{H}}(\mathbf{f})$ in the following quasi-Newton iteration:

$$\hat{\mathbf{f}}^{(n+1)} = \hat{\mathbf{f}}^{(n)} - \gamma \left[\tilde{\mathbf{H}}(\hat{\mathbf{f}}^{(n)}) \right]^{-1} \nabla J_m(\hat{\mathbf{f}}^{(n)}) \quad (14)$$

where γ is the step size. After substituting (12) into (14) and rearranging, we obtain our iterative algorithm

$$\tilde{\mathbf{H}}(\hat{\mathbf{f}}^{(n)})\hat{\mathbf{f}}^{(n+1)} = (1 - \gamma)\tilde{\mathbf{H}}(\hat{\mathbf{f}}^{(n)})\hat{\mathbf{f}}^{(n)} + \gamma 2\mathbf{T}^H\mathbf{g}. \quad (15)$$

We run the iteration (15) until $\|\hat{\mathbf{f}}^{(n+1)} - \hat{\mathbf{f}}^{(n)}\|_2^2 / \|\hat{\mathbf{f}}^{(n)}\|_2^2 < \delta$, where $\delta > 0$ is a small constant.

Equation (15) defines the iterate $\hat{\mathbf{f}}^{(n+1)}$ implicitly as the solution of a linear set of equations. The coefficient matrix $\tilde{\mathbf{H}}(\hat{\mathbf{f}}^{(n)})$ of this set is sparse, Hermitian and positive semi-definite, and hence these equations may themselves be efficiently solved using iterative approaches. To date, we have used the conjugate gradient (CG) algorithm for this solution, and terminated it when the ℓ_2 -norm of the relative residual becomes smaller than a threshold $\delta_{CG} > 0$ [45].

D. Auxiliary Processes

The structure of the above algorithm provides some insight into the expected feature-preserving behavior of the approach. For the sake of simplicity, let us assume that $\gamma = 1$. Then, the solution of (15) is also the minimizer of the following quadratic function with respect to \mathbf{f}

$$\begin{aligned} \|\mathbf{g} - \mathbf{T}\mathbf{f}\|_2^2 + \frac{k\lambda_1^2}{2}\mathbf{f}^H\mathbf{A}_1(\hat{\mathbf{f}}^{(n)})\mathbf{f} \\ + \frac{k\lambda_2^2}{2}\mathbf{f}^H\boldsymbol{\Phi}^H(\hat{\mathbf{f}}^{(n)})\mathbf{D}^T\mathbf{A}_2(\hat{\mathbf{f}}^{(n)})\mathbf{D}\boldsymbol{\Phi}(\hat{\mathbf{f}}^{(n)})\mathbf{f}. \end{aligned} \quad (16)$$

In this quadratic problem, $\mathbf{A}_j(\hat{\mathbf{f}}^{(n)})$ ($j = 1, 2$) act as spatially varying weighting matrices. The diagonal elements of these matrices correspond to auxiliary processes in the context of half-quadratic regularization. First consider the role of $\mathbf{A}_2(\hat{\mathbf{f}}^{(n)})$. At a location where there is an edge in the field, $(\mathbf{D}|\hat{\mathbf{f}}^{(n)})_i$ will be large, hence the corresponding element of $\mathbf{A}_2(\hat{\mathbf{f}}^{(n)})$ will be small, essentially suppressing the derivative penalty at that location through (16), and preventing smoothing across the edge. Similarly, elements of $\mathbf{A}_1(\hat{\mathbf{f}}^{(n)})$ provide weights which suppress energy constraints at locations where there is an object. Overall, the auxiliary processes associated with \mathbf{A}_1 and \mathbf{A}_2 can be viewed as foreground/background and edge maps respectively, and may be useful for interpretation of the formed image. Our algorithm generates these processes during the iteration process without any additional cost.

V. EXPERIMENTAL RESULTS

We demonstrate the effectiveness of our method on synthetic and real SAR scenes. We will show examples for both point-based feature enhancement and region-based feature enhancement, and compare these results to conventional reconstructions.

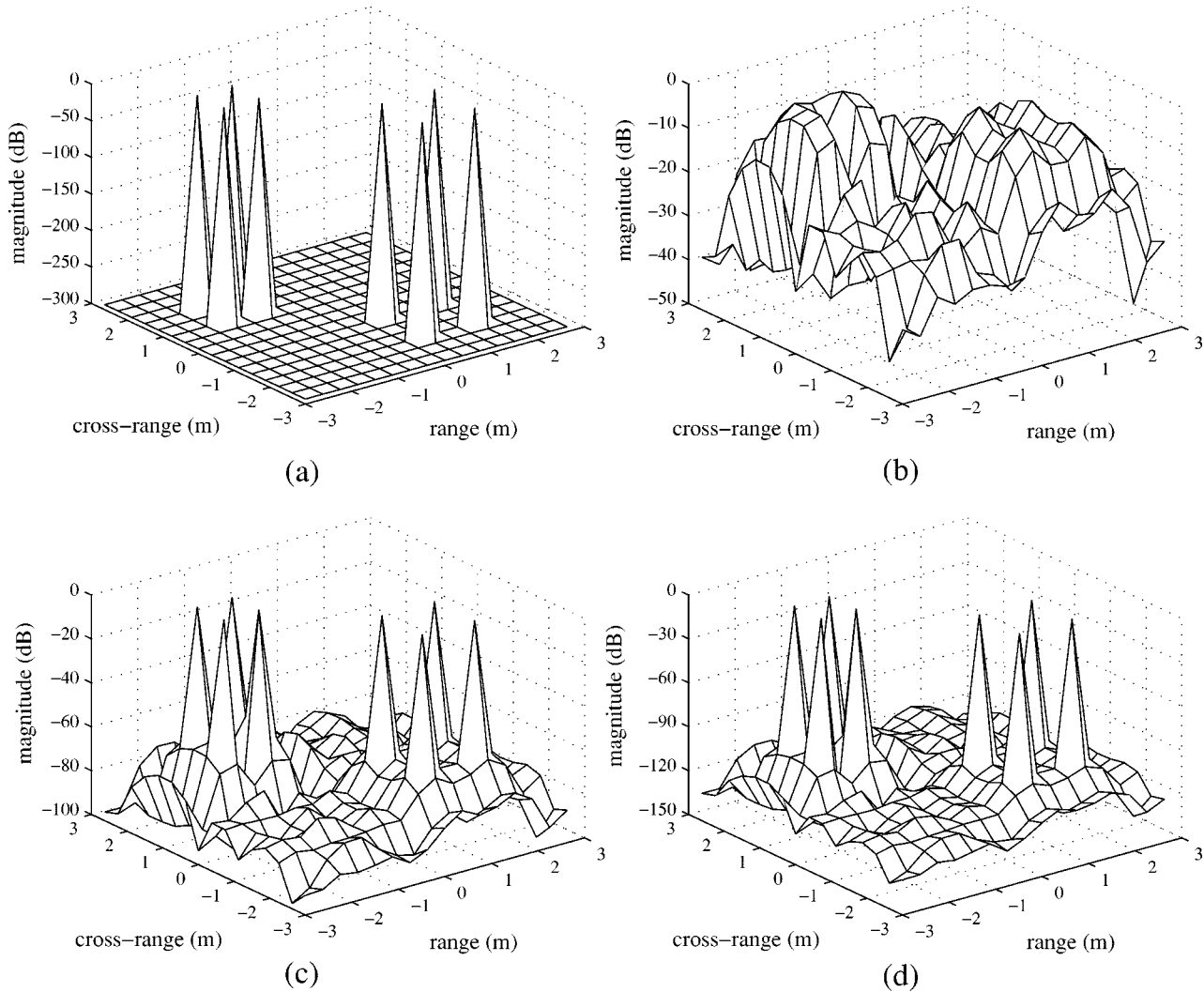


Fig. 3. Mesh plots of synthetic point scatterer reconstructions. (a) Truth. (b) Conventional method. (c) Proposed method with $k = 0.8$, $\lambda_1 = 1$, $\lambda_2 = 0$. (d) Proposed method with $k = 0.1$, $\lambda_1 = 1$, $\lambda_2 = 0$.

A. Algorithm Initialization and Parameter Selection

For all the examples, we initialize our algorithm with the conventional polar format reconstruction. Although the iterative scheme in (15) allows a variable step size, we use a fixed step size of $\gamma = 1$ in our examples. In our experience, the algorithm has always converged with this choice, hence varying (reducing) the step size has not been necessary. We set the approximation parameter in (10) to be $\epsilon = 10^{-5}$, which is small enough not to affect the behavior of the solution. For the termination conditions of (15), we use $\delta = 10^{-6}$ and a CG tolerance of $\delta_{CG} = 10^{-3}$. We choose the feature accentuation parameters λ_1 and λ_2 in (11) based on subjective qualitative assessment of the formed imagery, coupled with our imaging goals, as described below. Our experience on a large database of SAR images composed of similar scenes is that one set of parameters chosen on a single image can be used for the entire data set. In all the examples, we show the magnitude (in decibels) of the reconstructed complex-valued field. We increase the sparsity of $\tilde{\mathbf{H}}(\hat{\mathbf{f}}^{(n)})$ by neglecting elements in $\mathbf{T}^H \mathbf{T}$ whose magnitudes are smaller than 1% of the largest element.

B. Synthetic Scene Reconstructions

First, we demonstrate the superresolution capability of our method on a simple synthetic scene composed of eight single-pixel scatterers with unit reflectivity magnitude and random phase. The three-dimensional (3-D) mesh plot of the magnitude of this 16×16 pixel scene is shown in Fig. 3(a). We simulate SAR returns from this ideal scene such that the bandwidth of the data supports a resolution cell of 2×2 pixels. The conventional SAR reconstruction in Fig. 3(b) cannot resolve four of the scatterers falling into one resolution cell, and suffers from sidelobes. In this example, we want to accentuate points, hence we set $\lambda_2 = 0$ in (11). Fig. 3(c) and (d) show the results of our method with two different choices of k in (11). In these reconstructions, all the scatterers are resolved, background is suppressed, and peak reflectivity magnitudes are preserved [0.9552 in (c) and 0.9947 in (d)].

C. ADTS Data Reconstructions

We now show results on data from the MIT Lincoln Laboratory Advanced Detection Technology Sensor (ADTS) data set [46], [47]. Since the ADTS data set provides formed imagery

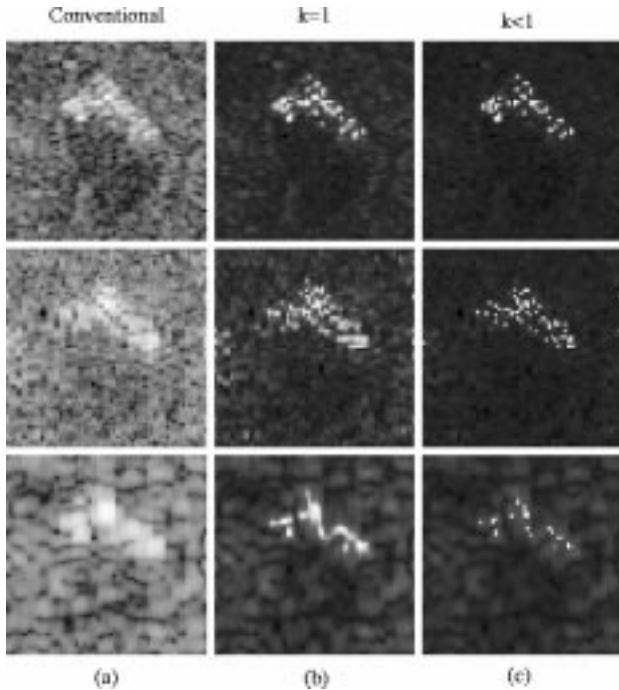


Fig. 4. Enhancement of point-based features. Resolution: top: 0.3 m, middle: 0.6 m, bottom: 1.2 m. (a) Conventional method. (b) Proposed method with $k = 1$, $\lambda_2 = 0$, and top: $\lambda_1 = 14$, middle: $\lambda_1 = 7$, bottom: $\lambda_1 = 10$. (c) Proposed method with $k < 1$ and $\lambda_2 = 0$, with top: $\lambda_1 = 14$, $k = 0.8$, middle: $\lambda_1 = 7$, $k = 0.8$, bottom: $\lambda_1 = 10$, $k = 0.95$.

only, we generate synthetic radar returns by computing Fourier transform samples on a polar grid and then using the resulting range profiles as the input to our reconstruction algorithm.

First, we show point-based feature enhancement results. In this example, all of the reconstructed images consist of 64×64 complex-valued pixels. Since we want to accentuate point features, we set $\lambda_2 = 0$ in (11). The top row in Fig. 4 contains 0.3 m resolution reconstructions of a scene containing an M48 tank. Our reconstructions appear to produce images with accentuated dominant peaks. Next, we reduce the bandwidth of the data equally in range and cross-range, and attempt to generate superresolution reconstructions. The middle and bottom rows in Fig. 4 contain reconstructions where resolution has been reduced to 0.6 m and 1.2 m, respectively. Although precise super-resolution arguments are not as easy for this complicated real SAR scene as for the synthetic scene of Fig. 3, the peaks still appear to be better localized by our approach. Note that a particular parameter choice in our method [such as that associated with the image in the bottom row of Fig. 4(b)] produces reconstructions which are visually very similar to the imagery obtained by the spectral estimation-based superresolution method of [19]. For a quantitative analysis of the improvements in scattering center locating accuracy provided by our technique, please see [48].

Now, we demonstrate formation of images with enhanced region-based features. Since we want to accentuate homogeneous regions, we set $\lambda_2 \geq \lambda_1$ in (11). Usually, we do not set $\lambda_1 = 0$, since we have observed that its presence helps in preserving the shadow regions. The images of this example consist of 128×128 complex-valued pixels. The top row in Fig. 5 contains ADTS images of an M48 tank reconstructed by using the conventional

method and by our proposed scheme for different choices of k . By choosing $k = 2$, our algorithm can produce reconstructions analogous to standard Tikhonov regularization, which we show for comparison. When $k \leq 1$, our method produces images where background fluctuations are suppressed, in contrast to the conventional image. Furthermore, this is achieved without compromising the sharp boundaries, unlike Tikhonov-type reconstructions. Similar observations apply to the reconstructions of a natural scene consisting of trees, two corner reflectors, fields and a road, shown in the bottom row of Fig. 5. Our method forms images in which the tree shapes and shadows are very distinguishable, and the background is quite smooth, whereas the conventional SAR image suffers from considerable amount of speckle.

D. URISD Reconstructions

Our final examples are from the XPATCH-generated University Research Initiative Synthetic Dataset (URISD) [49]. The URISD provides phase histories and range profiles, which we directly use as the input to our algorithm. Fig. 6 contains the CAD model of a fire truck used for data generation, and the corresponding reconstructed images. The conventional image in Fig. 6(b) suffers from large sidelobes. Sidelobes are conventionally suppressed by windowing the data prior to image formation, however this reduces the effective resolution in the formed image. Our reconstruction with a point-based prior is shown in Fig. 6(c), and achieves sidelobe suppression as well as increased resolvability of point scatterers. Our method with a region-based prior, on the other hand, produces an image with an enhanced object shape, as shown in Fig. 6(d).

VI. CONCLUSIONS

We have developed a method for complex-valued SAR image reconstruction which enhances features in the image. This is achieved by incorporating prior information about the behavior of the field and the features of interest into image formation through the minimization of an objective function. The resulting optimization problem is challenging, due to both the random-phase nature of the reflectivities, and the presence of nonquadratic functions of the field, which are needed for effective, robust feature enhancement. To address these issues, we have developed a new quasi-Newton method, built upon a half-quadratic-type regularization approach, which provides an efficient numerical solution to the optimization problem. This method is matched to the complex-valued nature of the SAR problem. Experimental results demonstrate the effectiveness of the proposed approach in forming SAR images with enhanced features and suppressed artifacts. Our method is generalizable to SAR scenarios requiring a more general observation model than that considered in this paper, and also to imaging problems other than SAR involving complex-valued quantities.

In this paper, we have concentrated on two types of features, and one family of functions (ℓ_k -norms) for the prior information terms. However, our framework and iterative algorithm remain valid for a wider range of potentially useful choices. This freedom could be exploited by letting a recognition system drive image formation by choosing the type of prior information terms

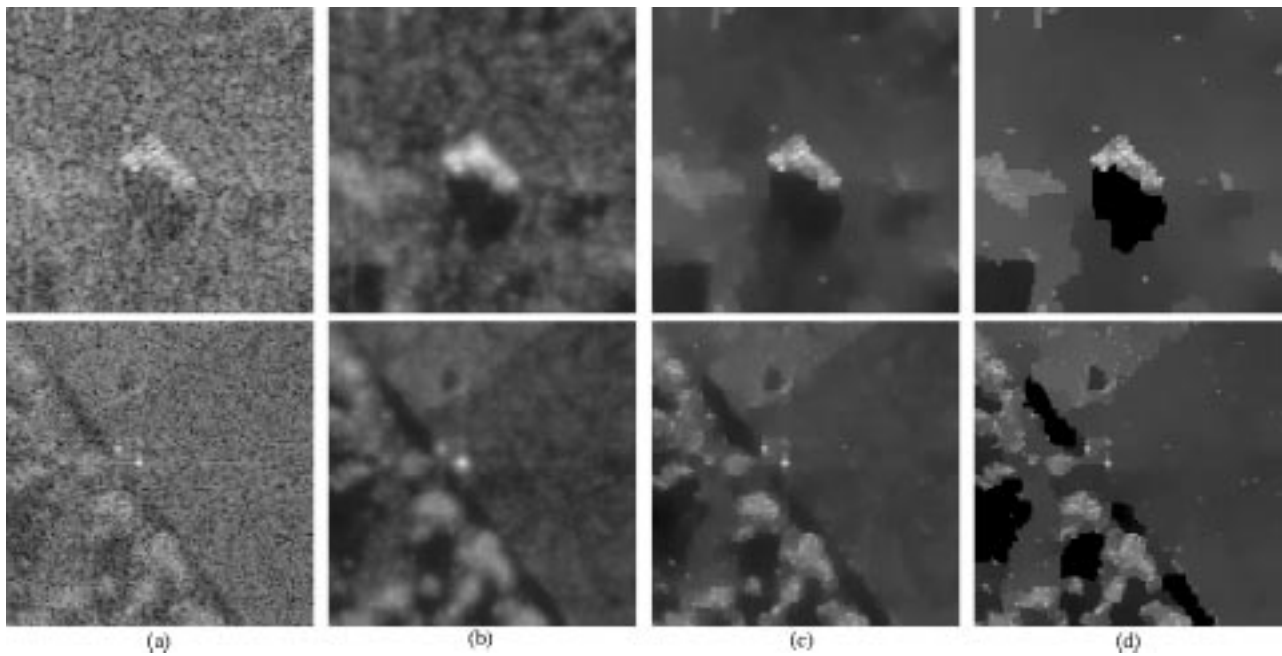


Fig. 5. Enhancement of region-based features. (a) Conventional method. (b) Tikhonov-type reconstruction (i.e., $k = 2$) with $\lambda_1 = 4$, $\lambda_2 = 22$. (c) Proposed method with $k = 1$, and top: $\lambda_1 = 5$, $\lambda_2 = 9$, bottom: $\lambda_1 = 4$, $\lambda_2 = 5$. (d) Proposed method with $k = 0.7$, and top: $\lambda_1 = 4$, $\lambda_2 = 6$, bottom: $\lambda_1 = 4$, $\lambda_2 = 4$.

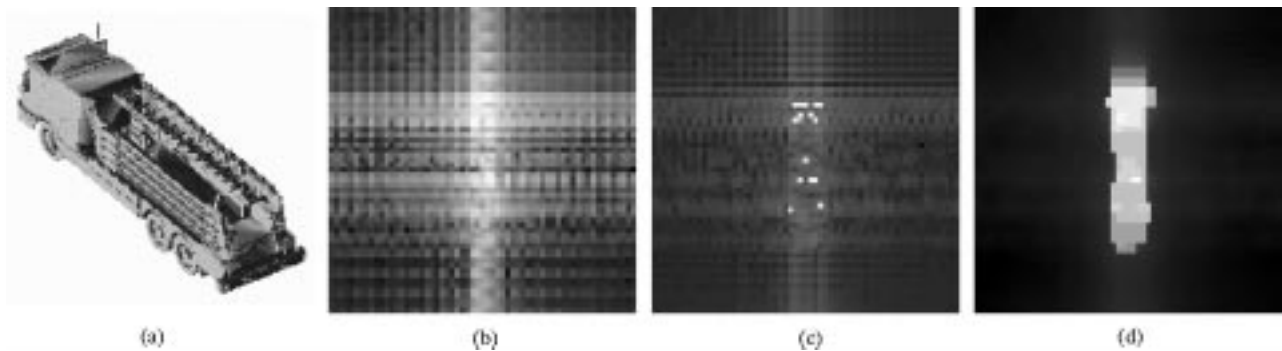


Fig. 6. Results with the URISD. (a) CAD model of the fire truck. (b) Conventional reconstruction. (c) Enhancement of point-based features with $k = 0.8$, $\lambda_1 = 22$, $\lambda_2 = 0$. (d) Enhancement of region-based features with $k = 0.8$, $\lambda_1 = 5$, $\lambda_2 = 9$.

to be used based on training data, such that recognition performance is optimized. Quantitative assessment of the impact of our approach on automatic recognition performance is a subject of our current research.

REFERENCES

- [1] W. G. Carrara, R. S. Goodman, and R. M. Majewski, *Spotlight Synthetic Aperture Radar: Signal Processing Algorithms*. Boston, MA: Artech House, 1995.
- [2] J. Walker, "Range-Doppler imaging of rotating objects," *IEEE Trans. Aerosp. Electron. Syst.*, vol. AES-16, pp. 23–52, Jan. 1980.
- [3] M. R. Banham and A. G. Katsaggelos, "Digital image restoration," *IEEE Signal Processing Mag.*, vol. 14, pp. 24–41, Mar. 1997.
- [4] C. R. Vogel and M. E. Oman, "Fast, robust total variation-based reconstruction of noisy, blurred images," *IEEE Trans. Image Processing*, vol. 7, pp. 813–824, June 1998.
- [5] P. Charbonnier, L. Blanc-Féraud, G. Aubert, and M. Barlaud, "Deterministic edge-preserving regularization in computed imaging," *IEEE Trans. Image Processing*, vol. 6, pp. 298–310, Feb. 1997.
- [6] A. H. Delaney and Y. Bresler, "Globally convergent edge-preserving regularized reconstruction: An application to limited-angle tomography," *IEEE Trans. Image Processing*, vol. 7, pp. 204–221, Feb. 1998.
- [7] D. L. Phillips, "A technique for the numerical solution of certain integral equations of the first kind," *J. Assoc. Comput. Mach.*, vol. 9, pp. 84–97, Jan. 1962.
- [8] A. N. Tikhonov, "Solution of incorrectly formulated problems and the regularization method," *Soviet Math. Dokl.*, vol. 4, pp. 1035–1038, 1963.
- [9] D. C. Munson, Jr. and J. L. C. Sanz, "Image reconstruction from frequency-offset Fourier data," *Proc. IEEE*, vol. 72, pp. 661–669, June 1984.
- [10] D. Geman and G. Reynolds, "Constrained restoration and the recovery of discontinuities," *IEEE Trans. Pattern Anal. Machine Intell.*, vol. 14, pp. 367–383, Mar. 1992.
- [11] D. Geman and C. Yang, "Nonlinear image recovery with half-quadratic regularization," *IEEE Trans. Image Processing*, vol. 4, pp. 932–946, July 1995.
- [12] C. V. Jakowatz, Jr., D. E. Wahl, P. H. Eichel, D. C. Ghiglia, and P. A. Thompson, *Spotlight-Mode Synthetic Aperture Radar: A Signal Processing Approach*. Norwell, MA: Kluwer, 1996.
- [13] D. C. Munson, Jr., J. D. O'Brien, and W. K. Jenkins, "A tomographic formulation of spotlight-mode synthetic aperture radar," *Proc. IEEE*, vol. PROC-71, pp. 917–925, Aug. 1983.
- [14] A. C. Kak and M. Slaney, *Principles of Computerized Tomographic Imaging*. New York: IEEE Press, 1988.
- [15] M. D. Desai and W. K. Jenkins, "Convolution backprojection image reconstruction for spotlight mode synthetic aperture radar," *IEEE Trans. Image Processing*, vol. 1, pp. 505–517, Oct. 1992.
- [16] C. W. Therrien, *Discrete Random Signals and Statistical Signal Processing*. Englewood Cliffs, NJ: Prentice-Hall, 1992.

[17] S. R. Degraaf, "SAR imaging via modern 2-D spectral estimation methods," *IEEE Trans. Image Processing*, vol. 7, pp. 729–761, May 1998.

[18] J. Li and P. Stoica, "An adaptive filtering approach to spectral estimation and SAR imaging," *IEEE Trans. Signal Processing*, vol. 44, pp. 1469–1484, June 1996.

[19] G. R. Benitz, "High-definition vector imaging," *Lincoln Lab. J.*, vol. 10, no. 2, pp. 147–170, 1997.

[20] S. Barbarossa, L. Marsili, and G. Mungari, "SAR super-resolution imaging by signal subspace projection techniques," in *Proc. Eur. Conf. Synthetic Aperture Radar*, Mar. 1996, pp. 267–270.

[21] D. C. Munson, Jr. and E. A. Ullman, "Support-limited extrapolation of offset Fourier data (synthetic aperture radar)," in *Proc. IEEE Int. Conf. Acoustics, Speech, Signal Processing*, Apr. 1986, pp. 2483–2486.

[22] H. Li, N. H. Farhat, and Y. Shen, "A new iterative algorithm for extrapolation of data available in multiple restricted regions with application to radar imaging," *IEEE Trans. Antennas Propagat.*, vol. AP-35, pp. 581–588, May 1987.

[23] I. J. Gupta, M. J. Beals, and A. Moghaddar, "Data extrapolation for high resolution radar imaging," *IEEE Trans. Antennas Propagat.*, vol. 42, pp. 1540–1545, Nov. 1994.

[24] I. J. Gupta and A. Gandhe, "Comparison of various enhanced radar imaging techniques," *Proc. SPIE*, vol. 3370, pp. 250–260, Apr. 1998.

[25] S. R. Degraaf, "SAR imaging via modern 2-D spectral estimation methods," *Proc. SPIE*, vol. 2230, pp. 36–47, Apr. 1994.

[26] J. A. C. Lee, O. Arikan, and D. C. Munson, Jr., "Formulation of a general imaging algorithm for high-resolution synthetic aperture radar," in *Proc. IEEE Int. Conf. Acoustics, Speech, Signal Processing*, vol. 4, Sept. 1996, pp. 2092–2095.

[27] C. L. Logan, "An estimation-theoretic technique for motion-compensated synthetic-aperture array imaging," Ph.D. dissertation, Mass. Inst. Technol., Cambridge, Feb. 2000.

[28] B. Borden, "Maximum entropy regularization in inverse synthetic aperture radar imagery," *IEEE Trans. Signal Processing*, vol. 40, no. 4, pp. 969–973, Apr. 1992.

[29] —, "Cross-entropy regularization and complex-valued image analysis applicable to ISAR," *Proc. SPIE*, vol. 2845, pp. 175–182, Aug. 1996.

[30] B. R. Frieden and A. T. Bajkova, "Entropic reconstruction of complex images," *Opt. Commun.*, vol. 102, no. 5–6, pp. 515–522, Oct. 1993.

[31] —, "Bayesian cross-entropy reconstruction of complex images," *Appl. Opt.*, vol. 33, no. 2, pp. 219–226, Jan. 1994.

[32] B. Borden, "Regularization of noisy ISAR images containing extended features," *IEEE Trans. Image Processing*, vol. 8, pp. 124–127, Jan. 1999.

[33] D. L. Mensa, *High Resolution Radar Imaging*. Dedham, MA: Artech House, 1981.

[34] L. C. Potter and R. L. Moses, "Attributed scattering centers for SAR ATR," *IEEE Trans. Image Processing*, vol. 6, pp. 79–91, Jan. 1997.

[35] G. Jones, III and B. Bhanu, "Recognition of articulated and occluded objects," *IEEE Trans. Pattern Anal. Machine Intell.*, vol. 21, pp. 603–613, July 1999.

[36] S. Sibisi, J. Skilling, R. G. Brereton, E. D. Laue, and J. Staunton, "Maximum entropy signal processing in practical NMR spectroscopy," *Nature*, vol. 311, pp. 446–447, Oct. 1984.

[37] R. Narayan and R. Nityananda, "Maximum entropy restoration in astronomy," *Ann. Rev. Astron. Astrophys.*, vol. 24, pp. 127–170, 1986.

[38] D. L. Donoho, I. M. Johnstone, J. C. Koch, and A. S. Stern, "Maximum entropy and the nearly black object," *J. R. Statist. Soc. B*, vol. 54, no. 1, pp. 41–81, 1992.

[39] P. Ciuciu, J. Idier, and J. F. Giovannelli, "Markovian high resolution spectral analysis," in *Proc. IEEE Int. Conf. Acoustics, Speech, Signal Processing*, vol. 3, Mar. 1999, pp. 1601–1604.

[40] C. Bouman and K. Sauer, "A generalized Gaussian image model for edge-preserving MAP estimation," *IEEE Trans. Image Processing*, vol. 2, pp. 296–310, July 1993.

[41] B. Bhanu, "Automatic target recognition: State of the art survey," *IEEE Trans. Aerosp. Electron. Syst.*, vol. AES-22, pp. 364–379, July 1986.

[42] J. A. Ratches, C. P. Walters, and R. G. Buser, "Aided and automatic target recognition based upon sensory inputs from image forming systems," *IEEE Trans. Pattern Anal. Machine Intell.*, vol. 19, pp. 1004–1019, Sept. 1997.

[43] D. G. Luenberger, *Linear and Nonlinear Programming*. Reading, MA: Addison-Wesley, 1989.

[44] C. R. Vogel and M. E. Oman, "Iterative methods for total variation denoising," *SIAM J. Sci. Comput.*, vol. 17, no. 1, pp. 227–238, Jan. 1996.

[45] G. H. Golub and C. F. Van Loan, *Matrix Computations*. Baltimore, MD: The Johns Hopkins University Press, 1996.

[46] Air Force Research Laboratory, Model Based Vision Laboratory, Sensor Data Management System ADTS. [Online] available: <http://www.mbvlab.wpafb.af.mil/public/sdms/datasets/adts/>.

[47] J. C. Henry, "The Lincoln Laboratory 35 GHz airborne polarimetric SAR imaging system," in *Proc. IEEE Nat. Telesyst. Conf.*, Mar. 1991, pp. 353–358.

[48] M. Çetin, W. C. Karl, and D. A. Castañon, "Evaluation of a regularized SAR imaging technique based on recognition-oriented features," *Proc. SPIE*, vol. 4053, pp. 40–51, Apr. 2000.

[49] Center for imaging science URISD Web page, http://cis.jhu.edu/wu_sensor_data/urisd/.



imaging.

Müjdat Çetin (S'98) received the B.S. degree from Boğaziçi University, İstanbul, Turkey, in 1993, and the M.S. degree from the University of Salford, Manchester, U.K., in 1995, both in electrical and electronic engineering. He is currently pursuing the Ph.D. degree at Boston University, Boston, MA.

He is currently a member of the Multidimensional Signal Processing Laboratory, Boston University. His research interests include statistical signal and image processing with an emphasis on inverse problems arising in remote sensing and medical



William Clem Karl (M'91–SM'00) received the Ph.D. degree in electrical engineering and computer science in 1991 from the Massachusetts Institute of Technology, Cambridge, where he also received the S.M., E.E., and S.B. degrees.

He held the position of Staff Research Scientist with the Brown-Harvard-MIT Center for Intelligent Control Systems and the MIT Laboratory for Information and Decision Systems, Cambridge, from 1992 to 1994. He joined the faculty of Boston University, Boston, MA, in 1995, where he is currently Associate

Professor of Electrical and Computer Engineering. Since January 1996 he has also held a joint appointment in the Department of Biomedical Engineering at Boston University. His research interests are in the areas of multidimensional and multiscale signal and image processing, geometric estimation, detection, and medical signal and image processing.

Dr. Karl was an Associate Editor of the IEEE TRANSACTIONS ON IMAGE PROCESSING from 1996 to 2000. He is a member of Sigma Xi. He has served in various organizational capacities, including as Session Organizer and Chair for the 2000 Conference in Information Sciences and Systems Special Session on Medical Imaging and as part of the organizing committee for the 1st SIAM Conference on the Life Sciences.